brain sciences

MDPI

Article

Selecting the Most Relevant Brain Regions to Classify Children with Developmental Dyslexia and Typical Readers by Using Complex Magnocellular Stimuli and Multiple Kernel Learning

Sara Mascheretti [1,*,†], Denis Peruzzo [2,†], Chiara Andreola [1,3], Martina Villa [1], Tommaso Ciceri [2], Vittoria Trezzi [1], Cecilia Marino [4,5] and Filippo Arrigoni [2,*]

1 Child Psychopathology Unit, Scientific Institute, IRCCS Eugenio Medea, 23842 Bosisio Parini, Italy; chiara.andreola@etu.u-paris.fr (C.A.); martina.villa@uconn.edu (M.V.); vittoriatrezzi@gmail.com (V.T.)
2 Neuroimaging Lab, Scientific Institute, IRCCS Eugenio Medea, 23842 Bosisio Parini, Italy; denis.peruzzo@lanostrafamiglia.it (D.P.); tommaso.ciceri@lanostrafamiglia.it (T.C.)
3 Laboratoire de Psychologie de Développement et de l'Éducation de l'Enfant (LaPsyDÉ), Université de Paris, 75005 Paris, France
4 The Division of Child and Youth Psychiatry at the Centre for Addiction and Mental Health (CAMH), Toronto, ON M6J 1H4, Canada; cecilia.marino@utoronto.ca
5 Department of Psychiatry, University of Toronto, Toronto, ON M5T 1R8, Canada
* Correspondence: sara.mascheretti@lanostrafamiglia.it (S.M.); filippo.arrigoni@lanostrafamiglia.it (F.A.)
† Both authors contributed equally to this work.

Abstract: Increasing evidence supports the presence of deficits in the visual magnocellular (M) system in developmental dyslexia (DD). The M system is related to the fronto-parietal attentional network. Previous neuroimaging studies have revealed reduced/absent activation within the visual M pathway in DD, but they have failed to characterize the extensive brain network activated by M stimuli. We performed a multivariate pattern analysis on a Region of Interest (ROI) level to differentiate between children with DD and age-matched typical readers (TRs) by combining full-field sinusoidal gratings, controlled for spatial and temporal frequencies and luminance contrast, and a coherent motion (CM) sensitivity task at 6%-CML6, 15%-CML15 and 40%-CML40. ROIs spanning the entire visual dorsal stream and ventral attention network (VAN) had higher discriminative weights and showed higher act1ivation in TRs than in children with DD. Of the two tasks, CM had the greatest weight when classifying TRs and children with DD in most of the ROIs spanning these streams. For the CML6, activation within the right superior parietal cortex positively correlated with reading skills. Our approach highlighted the dorsal stream and the VAN as highly discriminative areas between children with DD and TRs and allowed for a better characterization of the "dorsal stream vulnerability" underlying DD.

Keywords: developmental dyslexia; fMRI; multiple kernel learning; visual dorsal pathway; attention; dorsal stream vulnerability

check for updates

Citation: Mascheretti, S.; Peruzzo, D.; Andreola, C.; Villa, M.; Ciceri, T.; Trezzi, V.; Marino, C.; Arrigoni, F. Selecting the Most Relevant Brain Regions to Classify Children with Developmental Dyslexia and Typical Readers by Using Complex Magnocellular Stimuli and Multiple Kernel Learning. *Brain Sci.* **2021**, *11*, 722. https://doi.org/10.3390/brainsci11060722

Academic Editor: John F. Stein

Received: 7 April 2021
Accepted: 25 May 2021
Published: 28 May 2021

Publisher's Note: MDPI stays neutral with regard to jurisdictional claims in published maps and institutional affiliations.

1. Introduction

Developmental dyslexia (DD) is a complex heritable neurodevelopmental disorder characterized by impaired reading acquisition in spite of adequate neurological and sensorial functioning, educational opportunities, and average intelligence [1]. About 5%–12% of individuals are affected by this disorder, which incurs major lifelong disadvantages in educational and occupational attainment [2].

Reading is a complex task that is driven by neurobiological factors [3,4] and requires the coordination of multiple cognitive and perceptual systems [5,6]. The neurocognitive organization of reading ability depends on rapidly integrating a vast circuit of brain areas over the course of reading skill development. This "reading circuit" is made up of neural systems that support language as well as visual and orthographic processes, working memory,

attention, motor movements, and higher-level comprehension and cognition [2,5,7–9]. After initial processing of print occurs within the left-hemispheric fusiform gyrus (the visual word form area), a large left hemisphere circuit, including the supramarginal gyrus (orthography to phonology mapping), the superior temporal gyrus (phonological processing), the inferior parietal lobule and the angular gyrus (lexical-semantic processing) and the inferior frontal gyrus (phonological and semantic processing, working memory), is engaged [9–11]. Moreover, subcortical regions implicated in long-term and working memory, procedural learning and rapid sequential auditory processing (thalamus, basal ganglia and hippocampus) have also been implicated in reading [12–14]. Finally, the left and right fronto-parietal networks [15,16] strongly modulate both the visual and auditory word pathways by temporal and spatial selective attention [17]. As multiple cognitive and sensorial processes are involved in reading, it is probable that a widely variable pattern of weaknesses may contribute to reading difficulties across individuals [18]. While deficits in phonological awareness (i.e., the ability to isolate and manipulate sounds within words) are associated with and may have a causal role in DD [8,19], other theoretical models investigating deficits in underlying sensory (i.e., deficits in the auditory system [20–30]) and cognitive mechanisms (i.e., deficits in the rapid automatized naming [5,31], and in visual and auditory attention [32–38]) that potentially cause DD to remain compelling.

There is now a great deal of evidence supporting the role of the visual magnocellular (M) system in reading [39]. Reading requires the integration of two distinct neurocognitive systems: a visual system recognizes a visual word from within a crowded group of letters, and a phonological language system rapidly recognizes and produces spoken words from a group of phonemes [40]. The M and parvocellular (P) pathways are major parallel visual system streams that, along with the koniocellular system, constitute the sensory input and process all aspects of the visual world [41,42]. From the retina, the M and P ganglion cells project to different layers in the lateral geniculate nucleus (LGN), constituting the primary thalamic relay of parallel processing between the retina and visual cortex in the mammalian visual system [42,43]. Projections from the LGN remain partly segregated even beyond the primary visual cortex [44], where visual information flows onward along two separate pathways, i.e., the 'dorsal' and the 'ventral' visual streams, to several areas of the extrastriate visual cortex. In the dorsal stream, visual information flows directly from V1 to V5/MT+ and V6, and runs quite separately from these two areas through two channels, i.e., the ventro-dorsal (involving the inferior parietal lobule) and the dorso-dorsal (involving the superior parietal lobule, SPL) [45]. Visual information from V6 takes two different paths, i.e., the dorsolateral stream, which flows towards V5/MT+ and other areas of the extrastriate visual cortex (i.e., medial superior temporal area, V3A, V4T, ventral part the lateral intraparietal area), and the dorsomedial stream that runs towards the visuomotor areas of SPL (i.e., V6A, medial intraparietal area, ventral intraparietal area) [46]. The dorsal stream is considered blind to colors and responds optimally to contrast differences, low spatial frequencies, high temporal frequencies and real and illusory motion [47,48]. On the contrary, the ventral pathway goes from V1 sublayers 4Cβ, 4A, 3B and 2/3a through V2 and V4 to areas of the inferior temporal lobe (i.e., posterior inferotemporal, central inferotemporal and anterior inferotemporal). This stream is especially associated with stimuli involving color and form, high spatial frequency, low temporal frequency and low luminance contrast [48].

The visual M system contributes to promptly recognizing and sequencing letters. The former happens by rapidly focusing the ventral attention network (VAN) on the letter to be identified, while the latter happens by logging the amplitude and the order of attentional shifts and eye movements during the inspection of each word [32,33,38,49,50]. As the dorsal visual stream is intimately related to attentional systems and particularly to areas shown to be involved in attention control [51,52], the M system plays a vital role in controlling the sequential allocation of attention for reading (attentional shifting) [38,47,53–55]. According to the "sluggish attentional shifting" (SAS) hypothesis [32], shifting attention from one object to another is impaired in subjects with DD; is one of the most important predictors

of early reading abilities; is a specific target in training that significantly improve reading skills [47]. Therefore, it is plausible to hypothesize that a weakened or abnormal M input in the dorsal visual stream, and the consequent dysfunction of the main fronto-parietal attentional network, could be a neurobiological substrate of SAS in DD [53,54].

Sinusoidal gratings and sensitivity for motion coherence are two classic psychophysical visual tasks [56] that have been widely employed to investigate the neural correlates of the dorsal and ventral visual pathways in the general population [42,43,57–64] and in subjects with DD [44,58,65–67], as they tap the psychophysical characteristics of the two cell classes (i.e., M and P) involved in the two visual pathways [68].

Several lines of evidence have shown deficits in the M visual pathway in subjects with DD [69], including abnormally small cells in the M layers of the lateral geniculate nuclei of the thalamus [70,71], impaired perceptual performance [72–83] and reduced electrophysiological responses to stimuli mainly processed by the M pathway [53,84–86]. However, subjects with DD perform normally on visual tasks preferentially associated with the P pathway [87]. By translating sensory performance into brain functioning, five functional brain imaging studies have revealed reduced or absent activation in areas within the visual M pathway in four independent samples with DD [44,58,65–67], although other studies have reported negative findings [88,89]. In particular, Eden and colleagues found no activation in V5/MT during a coherently moving, low-contrast (5%), random-dot stimulus (100% coherence) in eight adults with DD compared to eight typical readers (TRs) [44]. While processing a random-dot stimulus, children with DD showed higher activation in the right inferior and middle frontal gyri ($p < 0.05$ FWE cluster corrected) and reduced activation in the bilateral visual cortex (including V5/MT+; $p < 0.05$ uncorrected) compared to age-matched TRs [58]. Likewise, Olulade and colleagues reported that V5/MT activity was greater for the age-matched TR group than for children with DD (p-value = 0.001) during suprathreshold coherent motion (CM) detection (40% coherence) [67]. By using sinusoidal gratings, young adult individuals with DD showed lower activation in both bilateral V1 and MT+ compared to young adult TRs across the full range of contrasts [65,66]. Interestingly, differences in activation within these areas positively correlated with individual differences in reading rate [65,66].

Understanding the role of the visual M pathway in DD and in higher-order cognitive mechanisms related to DD (i.e., attentional shifting) is critical to the early identification and successful treatment of reading disability. Previous fMRI studies have primarily addressed the role of only a few specific brain regions involved in visual motion perception. However, the visual system receives stimulus-driven (bottom-up) as well as a goal-directed (top-down) attentional influence, which modulates all visual processing levels from V1 to visual word form area [15–17,38,90]. Investigating this complex pathway presents three challenges. First, previous neuroimaging studies primarily employed univariate analysis to investigate group differences in the primary visual cortex and extrastriate areas. Univariate analysis is the simplest approach for neuroimaging statistical analysis, as it deals with each region (or image voxel) independently from each other. Thus, it investigates just the direct relationship between DD and the single region, without considering the nature of interdependencies between brain regions underlying the visual M stream and the brain regions sensitive to the associated M demands [44,58,65–67]. Processing M stimuli activates an extensive brain network that is difficult to characterize when accounting for only a few occipital brain regions. Therefore, the univariate analysis does not enable us to explore the integrated activation of multiple brain regions (i.e., the dorsal visual stream and the attentional systems), nor to investigate group differences. Second, previous imaging studies employed visual tasks controlled for only one functional feature at a time (i.e., spatial or temporal frequencies, or luminance contrast) and often adopted suprathreshold stimuli [44,58,67]. It has been argued that the use of these visual stimuli failed to assess the integrity of the visual streams [42,91]. Previous evidence suggests an advantage in simultaneously manipulating more than one functional feature (e.g., both spatial and temporal frequencies) of the visual stimulus and in using stimuli at both threshold and suprathreshold levels to achieve a better

characterization of the visual streams' responses across the brain [15,16,42,43,64,92–99]. There are two possible interpretations of the threshold in the visual system [100]: (1) the threshold is the minimum level of physical stimulus that can generate output from the sensory process (cf. the high-threshold model) [101]; and (2) the threshold is the physical stimulus that yields a criterion level of performance (cf. the signal detection model) [102]. Third, previous studies have had relatively small samples (adults with DD n = 6 and adult TRs n = 8 [44]; adults with DD n = 5 and adult TRs n = 5 [65,66]; children with DD n = 14, age-matched TRs n = 14 and reading-matched TRs n = 10 [67]), and few neuroimaging studies have directly investigated group differences in the visual M pathway in children with DD [58,67]. These do not provide a reliable account of the mechanisms underlying group differences in visual M stream functioning during development.

To address the above concerns, the present study aimed to investigate whether TRs and children with DD showed different neural activation during two well-established fMRI visual tasks, (1) full-field sinusoidal gratings, in which we simultaneously manipulated spatial and temporal frequencies and luminance contrast close to threshold levels; and (2) sensitivity to motion coherence for both threshold and suprathreshold levels. Whole-brain multivariate analyses implemented through a multiple kernel learning (MKL) machine [103] were used to identify the brain regions sensitive to M stream demands and relevant to the classification task. While univariate methods identify regions especially responsive to different stimulus properties (e.g., low versus high spatial frequency) within the visual M stream, the MKL method assists the execution of a whole-brain multivariate analysis without relying on any a priori assumptions regarding the role of key brain regions in the visual M stream. Thus, this analysis enables the detection of a sparse brain model based on a subset of brain regions that significantly contribute to the visual M stream.

2. Materials and Methods

The protocol was approved by the Scientific Review Board and the Ethical Committee of the Scientific Institute, IRCCS Eugenio Medea.

2.1. Participants

Twenty-five children with DD (age = 13.92 ± 1.58; 6 females) and 24 TRs (age = 13.13 ± 1.63; 8 females) took part in the present study. Children with DD were recruited from an ongoing project about the genetic basis of DD [104]. Subjects were included if they had a clinical diagnosis of DD [105]. TRs were recruited via 2 different ascertainment schemes: (1) children were contacted by word of mouth among students attending middle and high schools in two districts in northern Italy, i.e., Milan and Lecco; (2) children were selected from a community-based cohort of 819 Italian children aimed at investigating the effects of both genetic and environmental risk factors upon behavioral, cognitive and linguistic measures [106]. For both general population samples, inclusion criteria were: (i) belonging to Caucasian families who were at least first-generation native Italian speakers; (ii) having no certified neurological, neurodevelopmental, visual, hearing, intellectual or motor disabilities; and (iii) having written informed consent signed by both parents.

2.2. Neuropsychological Assessment

Both TRs and children with DD underwent the following assessments:

(1) IQ, as estimated by the vocabulary and block design subscales of the WISC-III [107];
(2) Reading, as assessed by text [108,109], single unrelated words and pseudo-words reading tests [110,111];
(3) Verbal working memory (VWM), as assessed by the Single Digit Forward Span, Single Digit Backward Span, Single Letter Forward Span, and Single Letter Backward Span tasks [112];
(4) Phonological skills, as assessed by the nonword repetition test (NWR) [113];
(5) Hand preference, as assessed by the Briggs and Nebes Inventory (BNI) [114];

(6) ADHD traits, as assessed by the Conners' Parent Rating Scales–Revised:Long version (CPRS-R:L) [115–117]. For the current purpose, two subscales were considered: DSM-IV-inattention (DSM-IV-I) and DSM-IV-hyperactivity/impulsivity (DSM-IV-HI).

To be included, both TRs and children with DD were required to have a mean score between vocabulary and block design subtests of the WISC-III of $\geq$7 (i.e., ≥ -1.00 SD) [107], no other neuropsychiatric diagnoses, no major contraindications to MRI, and normal or corrected-to-normal vision. Children with DD were included if they had either accuracy or speed z-score of ≤ -2.00 SDs on text or single unrelated words or pronounceable pseudo-words reading tests. TRs were included if they had both accuracy and speed z-scores of ≥ -1.00 SD on all reading tests.

Table 1 shows the descriptive statistics of demographic and neuropsychological variables of both DD and TR groups after the fMRI data quality check (cf. '2.6 fMRI data processing' paragraph). As expected, children with DD showed significantly lower scores in all reading tests compared to TRs. To control for confounders, block design and DSM-IV-I were entered as covariates in subsequent analyses of imaging data processing (cf. '2.6 fMRI data processing' paragraph). Regarding IQ, we decided to control only for block design because several previous cross-sectional and longitudinal studies reported a relationship between reading skills and verbal IQ [118–123]. Moreover, as mean bivariate correlations (r) were substantial within reading and VWM tests (reading r = 0.766, Supplementary Table S1a; VWM r = 0.391, Supplementary Table S1b), we created two composites by averaging each task within reading and VWM.

2.3. MRI Acquisition Protocol

MRI data were acquired on a 3T Philips Achieva d-Stream scanner (Best, The Netherlands) with a 32-channel head coil. Visual stimuli were developed with Presentation® software (Neurobehavioral System Inc., Berkeley, CA, USA) and delivered through a VisuaStim digital device for fMRI (Resonance Technology Inc., Northridge, CA, USA). MRI-compatible goggles with two displays were used, with a 60 Hz frame rate and 800 × 600 spatial resolution (4/3 aspect ratio) subtending a horizontal visual angle of 30°. An MRI-compatible pad was used to record subjects' answers and response times. The MRI protocol included the use of an anatomical T1-weighted (T1W) 3D Turbo Field Echo sequence as a subject morphological reference of MRI data (Field Of View (FOV) = 256 × 256 × 175 mm^3, voxel size 1 × 1 × 1 mm^3, Time of Repetition (TR) = shortest (~8.1 ms), Time of Echo (TE) = shortest (~3.7 ms), Flip Angle (FA) = 8°). The fMRI data were acquired with a T2*-weighted Gradient Echo planar sequence (FOV = 240 × 240 mm^2, voxel size = 3 × 3 mm^2, slice thickness = 3 mm, slice gap = 0.5 mm, slice number = 39, TR = 2 s, TE = 26 ms, FA = 90°).

Table 1. Descriptive statistics of demographic and neuropsychological variables.

		Children with DD (n = 22)					Typical Readers (n = 22)					X^2	df	*p*
Sex (Male/Female)				16/6					15/7			0.11	1	0.741
Handedness	**Right-handed**			18					17					
	Left-handed			3					3			0.31	2	0.856
	Ambidextrous			1					2					
		Min	**Max**	**Mean (SD)**	**Skewness**	**Kurtosis**	**Min**	**Max**	**Mean (SD)**	**Skewness**	**Kurtosis**	***t*-Test**	**df**	***p***
Age		10.92	16.5	14.10 (1.48)	−0.40	−0.22	11	16.25	13.18 (1.65)	0.47	−1.31	−1.94	42	0.059
IQ †		7.0	13.5	10.59 (1.78)	−0.10	−0.61	7.5	18.5	13.70 (2.82)	−0.67	0.23	4.38	42	<0.001
IQ, Vocabulary		5.0	16.0	9.73 (2.75)	0.25	−0.24	8.0	18.0	13.23 (3.09)	−0.27	−0.95	3.98	42	<0.001
IQ, Block Design		8.0	18.0	11.82 (2.04)	1.16	3.10	7.0	19.0	14.18 (3.65)	−0.47	−0.49	2.65	42	0.012
TR, accuracy		−10.43	0.74	−3.34 (2.42)	−1.30	2.52	−0.13	1.42	0.61 (0.34)	0.10	0.88	7.61	42	<0.001
TR, speed		−4.21	−0.09	−2.55 (1.01)	0.44	−0.11	−1.00	1.18	0.16 (0.65)	0.02	−1.00	10.55	42	<0.001
SWR, accuracy		−10.00	0.33	−3.41 (2.63)	−0.74	0.22	−0.67	1.00	0.27 (0.56)	−0.04	−1.16	6.42	42	<0.001
SWR, speed		−10.12	−0.41	−3.66 (2.16)	−1.49	2.77	−1.11	0.87	0.04 (0.57)	−0.19	−0.96	7.75	42	<0.001
SPWR, accuracy		−8.50	0.33	−2.28 (1.91)	−1.57	4.33	−0.67	1.33	0.50 (0.46)	−0.47	0.60	6.61	42	<0.001
SPWR, speed		−9.42	−0.67	−3.38 (2.42)	−1.43	1.36	−1.03	1.40	0.26 (0.64)	−0.26	−0.65	6.82	42	<0.001
SLFS		−2.30	0.65	−1.15 (0.72)	0.46	0.61	−1.35	1.35	0.14 (0.76)	−0.69	−0.28	5.72	41	<0.001
SLBS		−2.20	1.35	−0.71 (0.75)	0.93	2.25	−1.35	1.60	−0.07 (0.89)	0.73	−0.41	2.53	41	0.015
SDFS		−2.20	0.00	−1.38 (0.62)	0.49	−0.08	−2.00	1.00	−0.61 (0.74)	0.18	−0.21	3.68	41	0.001
SDBS		−1.35	0.65	−0.56 (0.47)	0.56	1.01	−1.40	2.00	0.10 (0.96)	0.91	−0.20	2.84	41	0.007
SNWR		−7.00	3.53	−1.66 (2.71)	−0.1	−0.41	−2.79	3	1.18 (1.40)	−1.45	2.26	4.38	42	<0.001
ADHD	**DSM-IV-I** ‡	41	82	60.09 (10.73)	0.33	−0.32	39	59	46.11 (5.49)	0.94	0.34	−5.43	42	<0.001
	DSM-IV-HI §	38	71	49.20 (7.96)	1.13	1.57	38	65	47.36 (7.63)	1.099	0.377	−0.76	40	0.450
SES ¶		20	90	58.84 (19.16)	−0.08	−0.37	30	90	60.23 (19.42)	0.19	−1.04	0.56	39	0.579

TR: Text reading; SWR: single words reading; SPWR: single pseudo-words reading; SLFS: single letters forward span; SLBS: single letters backward span; SDFS: single digits forward span; SDBS: single digits backward span; SNWR: single non-word repetition. † Mean score of vocabulary and block design subtests of the WISC-III [108]. ‡ The DSM-IV-Inattention (DSM-IV-I) subscale of the CPRS-R:L [116–118]. § The DSM-IV-hyperactivity/impulsivity (DSM-IV-HI) subscale of the CPRS-R:L [116–118]. ¶ As estimated by father's/mother's employment [124].

2.4. fMRI Task Design

2.4.1. Full-Field Sinusoidal Gratings

The task consisted of 14 s blocks of "M stimuli," "P stimuli" and blank stimuli (fixation point only). The M and P stimuli were designed to elicit differential bold responses from M and P pathways [43]. The M stimulus was a monochrome, low spatial frequency, high temporal frequency, high luminance contrast, full-field sinusoidal grating with sinusoidal counterphase flicker; the P stimulus was a high color contrast, high spatial frequency, low temporal frequency, low luminance contrast full-field sinusoidal grating with sinusoidal counterphase flicker. The M stimulus was a 100% luminance contrast, black–white grating with a spatial frequency of 0.5 cycles per degree (cpd) and a flicker frequency of 15 Hz. The P stimulus was a low luminance contrast, high color contrast red–green grating with a spatial frequency of 2 cpd and a flicker frequency of 5 Hz. Color levels in the P stimulus were set to be near-isoluminant, the red luminance was set to the maximum level, and the green was set to 39% of the maximum level, as implemented in Denison and colleagues [43]. The blank stimulus was a gray screen of mean luminance. The outer borders of each stimulus faded into gray to avoid sharp visual edges at the stimulus boundaries. Both gratings were presented at one of 6 orientations (0°, 30°, 60°, 90°, 120° and 150°) and changed to the next orientation every 2.33 s. The protocol included 28 blocks (8 M, 8 P and 12 blank) presented in pseudorandom order with the constraint that the same stimulus type could not appear in adjacent blocks to minimize adaptation to the stimuli. A white fixation point subtending 0.2° visual angle appeared at the center of the screen throughout the stimulus blocks. Subjects were instructed to maintain fixation throughout the run, and they performed an irrelevant target detection task during the M and P stimulus blocks to encourage them to do so. The target was a bidimensional Gaussian contrast reduction patch. Its size was linearly scaled with the distance from the fixation point. The target appeared for 300 ms at random times and in random positions 50% of the time during the second half of each stimulus block. At the end of each stimulus block, the screen turned gray, and subjects were asked to press the corresponding button in the response pad to answer questions (i.e., "Did the target appear?"—right button for "Yes" and left button for "No"). Subjects had 4s to answer the question. There was a 2s inter-stimulus waiting period between stimulus blocks.

2.4.2. CM Detection

Sensitivity to motion coherence was assessed for radial motion (expanding or contracting), which has previously proved able to evoke more activation than simple coherent motion (i.e., vertical/horizontal) [57,125], and which made it easy for subjects to maintain fixation [95]. The stimuli comprised 50 small white and 50 small black dots (each 20 arcmins), presented for 250 ms on a mean luminance gray background. A proportion of dots drifted coherently at a speed of 10°/s (limited lifetime of 8 frames, frame rate 60 Hz), while the remainder were displayed in random positions on each frame. According to previous studies on children with and without neurodevelopmental disorders [63,67,93,94,125,126], we used three levels of coherently moving dots (CML: Coherent Motion Level), i.e., 6%, 15% and 40%. At the beginning of each stimulation block, a white fixation point subtending 0.2° visual angle appeared at the center of the screen for 0.5 s and was followed by the 0.25 s CM stimulus. Subjects were instructed to maintain fixation throughout the run, and were actively engaged in performing a motion detection task and pressing the corresponding button on the response pad to answer questions (i.e., right button for expanding and left button for contracting). After the stimulus, subjects had 4 s to answer the question and were asked to give an answer even when they could not detect the motion direction. There was a 4.25 s inter-stimulus waiting period between stimulus-blocks. The protocol included 48 stimuli (8 repetitions for each combination of coherence level and motion direction) administered in a pseudorandom order with the constraint that the same coherence level could not appear in more than two adjacent blocks regardless of the motion direction.

2.5. Anatomical MRI Data Analysis

T1W images were corrected for bias field intensity artifacts using the N4 algorithm [127]. Subsequently, FreeSurfer tools (http://surfer.nmr.mgh.harvard.edu/, version 6.0) were used to further process the T1W images following the recon-all processing pipeline. The HCP-MMP1 atlas was used to divide each hemisphere into 180 regions, which can be grouped into 22 macro-regions [128].

2.6. fMRI Data Processing

The fMRI data were processed following the FreeSurfer Functional Analysis Stream (FSFAST, version 6.0). The preprocessing pipeline included motion correction, slice-timing correction, resampling on the 'fsaverage' template, smoothing, and intensity normalization. Template resampling was performed by exploiting the subject T1W images as an intermediate step, and smoothing was performed using a 3 mm FWHM filter.

Outlier volume detection was performed using an ad-hoc software we made by selecting all the volumes with (1) an overall motion from the previous volume larger than 2 mm, or (2) a mean intensity difference from the previous volume larger than 2.5 times the standard deviation in the whole run. The fMRI runs were excluded from the study if more than 20% of their overall volume was tagged as an outlier or if more than 30% of their volume was tagged as an outlier for a single stimulus condition. This led to the exclusion of three children with DD (all males) and two TRs (one male). The excluded subjects did not differ from the included ones in any of the selected demographic or neuropsychological variables (data available upon request). The final groups had 22 subjects each. The number of outlier volumes for each task of each included subject did not significantly differ between the groups (full-field sinusoidal gratings, p-value = 0.34; CM detection, p-value = 0.42).

For each subject, a first-level analysis was performed with a GLM model using the task conditions as predictors of interest and the motion parameters and outlier volumes as nuisance predictors. Subsequently, contrast maps were defined within each task. Regarding the full-field sinusoidal gratings, two contrast maps were specified, i.e., M stimulus vs. Baseline (M-*vs*-B) and P stimulus vs. Baseline (P-*vs*-B). Three contrast maps were outlined for the coherent motion, one for each level of motion coherence, i.e., Coherent Motion Level 6% vs. Baseline (CML6-*vs*-B), CML15-*vs*-B, CML40-*vs*-B. Finally, each contrast map was partitioned into Regions of Interest (ROI), which is an approach that extracts data from a subset of voxels belonging to a homologous anatomo-functional brain region, improving the signal-to-noise ratio. In particular, the mean value of each contrast map was computed for each subject in the cortical ROI from the HCP-MMP1 atlas by using a linear model that allowed to control for the effects of performance IQ and DSM-IV-I in order to remove the amount of the signal explained by these confounders from our dependent variable (i.e., the mean value of each contrast map) (see Supplementary Figure S1 for a flowchart of the pipeline).

2.7. Multivariate Analyses

A machine learning-based analysis was performed on the ROI data (controlled for the effects of performance IQ and DSM-IV-I) to investigate whether visual fMRI tasks can be used to discriminate between TRs and children with DD and to detect which ROIs contribute most to the classification.

In the classification experiments, we used a multiple kernel technique [129,130] based on the Support Vector Machine (SVM) model to combine multiple contrast maps while preserving the topological information (see Supplementary Figure S2 for a flowchart of the classification experiment). In the SVM model, we included a weight for each kernel learned during the training (higher weights were assigned to the kernels providing the largest discriminative information). As a different linear kernel was associated with each ROI, the kernel weights quantified the contribution of each ROI to the final classification and could be interpreted as ROI weights. Moreover, for each ROI, the mean values from the different contrast maps were concatenated in a single input vector, thus preserving the topological

information among the tasks. In this study, we employed the Group Lasso–Multiple Kernel Learning algorithm (GL–MKL) [131], which included a sparsity contribution to the regulation term during the kernel weights training procedure. The sparsity parameter (p) and the SVM error penalty parameter (C) were estimated by adopting a grid search approach and a double cross-validation procedure to avoid overfitting. More precisely, in each iteration of the outer cross-validation cycle, two subjects, one DD and one TR, were used as a testing set to avoid the anticorrelation effect with the training set [132]. In the inner cross-validation cycle, a ten-fold cross-validation procedure was used to optimize the classifier parameters. Classifier performances were evaluated using classification accuracy, the area under the ROC curve (AUC) and the *p*-value. The *p*-value was computed using a permutation test with 10,000 permutations of the subject labels.

Theoretically, all ROIs contributed to the classification task; thus, we performed an analysis to identify the subset of ROIs that contributed the most to the classification. Following a Greedy backward elimination approach [133], we fixed the model parameters (C, *p*-value) to the consensus values derived from the cross-validation procedure, and we iteratively backward removed the ROI with the lowest weight and retrained the classifier. We selected the configuration with the best performance (i.e., accuracy, AUC) and extracted the set of ROIs that best differentiated between TRs and children with DD. As the magnitude of the SVM weights associated with each feature did not have a direct neurophysiological interpretation, linear backward models were transformed into forward models [134]. In each forward model, a weight (contrast weight) was associated with each element of the input vector (i.e., the ROI contrast values) and could be interpreted as generative models (e.g., GLM). Contrast weights indicated the contribution of the target class (i.e., DD) to each element of the feature vector (i.e., the value of each contrast map activation in the given ROI) and were used to identify which task held the largest discriminative information within each ROI.

As contrast weight analysis is influenced by the complementary information provided by the different contrasts in the selected ROIs, we performed univariate post hoc analyses (i.e., *t*-tests) to independently investigate the direction and magnitude of the differences between TRs and children with DD for each contrast.

Correlations between the mean activation of each contrast map (i.e., M-*vs*-B, P-*vs*-B, CML6-*vs*-B, CML15-*vs*-B and CML40-*vs*-B) within the significant ROIs and the neuropsychological domains (i.e., reading, VWM and phonology) in the total sample were calculated using Pearson correlations as implemented in IBM SPSS Statistics for Windows, Version 21.0 (IBM Corp. Released 2012).

To summarize, the whole multivariate analysis can be broken down into four steps: firstly, we performed a classification experiment to discriminate between TRs and children with DD by using whole-brain ROIs. Secondly, we performed an analysis on the selected classifier to identify which ROIs and contrast maps contributed most to the classification. Thirdly, we ran univariate post hoc analyses (i.e., *t*-tests) to investigate the direction and the magnitude of the differences between TRs and children with DD in the selected ROIs. Finally, we tested for correlations between task-induced cortical activation in the different ROIs and the neuropsychological tests.

3. Results

Multivariate Analyses—The Group Lasso–Multiple Kernel Learning Algorithm

Using the GL–MKL on the HCP-MMP1-defined ROIs for all contrast maps resulted in a model which discriminates between TRs and children with DD with 65.9% accuracy and 64.7% AUC (*p*-value = 0.043). On the basis of the post hoc ROI weight analysis (see "Section 2.7"), we identified a set of 11 ROIs that were likely to have contributed most to the classification (Figure 1).

Figure 2 shows the ranking of the selected ROIs and the corresponding ROI-weight.

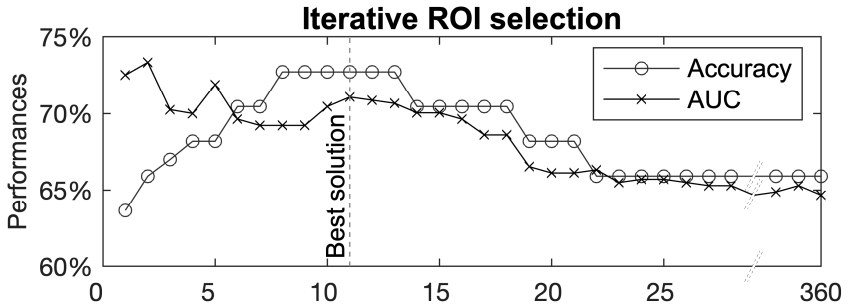

Figure 1. Post hoc analysis to select the subset of ROIs that contributed most to the classification. The *X*-axis reports the number of ROIs used for the classification. The *Y*-axis reports classification performance scored with that set of ROIs. ROIs are iteratively removed from the lowest to the highest weight, which was assigned by assessing all of them. The red dashed line indicates the best configuration.

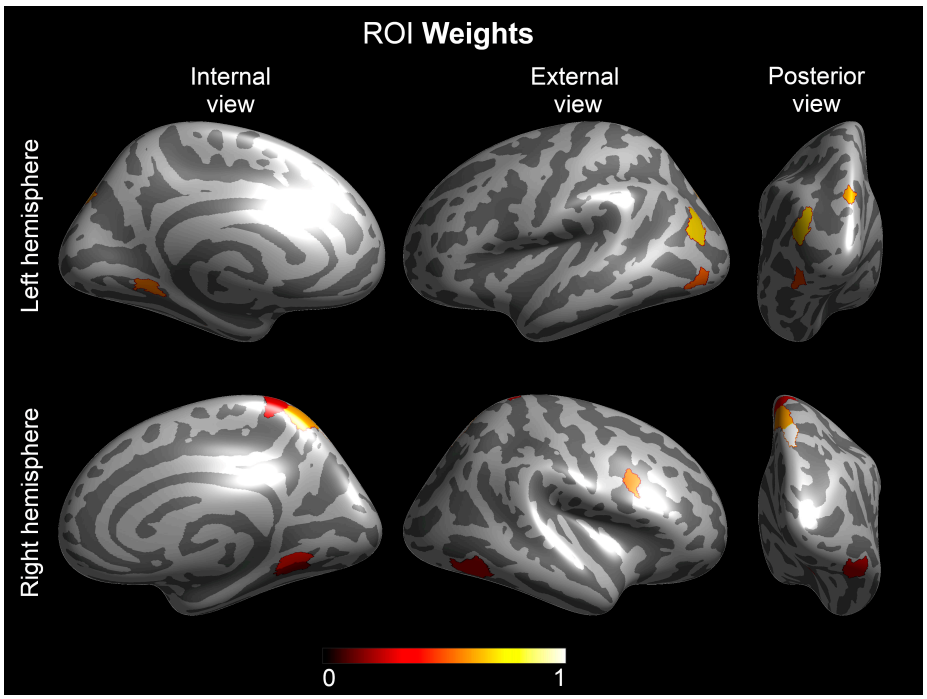

Figure 2. ROI weights for the 11 ROIs that provide the highest GL–MKL classifier performance. ROIs from the HCP-MMP1 atlas [128] were selected by the MKL to classify TRs and children with DD. ROI weights were scaled to a maximum value equal to 1, and the color of the regions varies from black (minimum ROI weight) to white (maximum ROI weight).

Table 2 reports the ROI weights and the contrast weights obtained with the forward model. Univariate post hoc statistical analyses at the ROI level for each contrast are reported in Table 3. Although none of the *t*-tests survived a whole-brain multiple comparison correction, the qualitative interpretation of the *t*-values provides useful information about the group differences, which are complementary to the significant results obtained with the multivariate analysis. Almost all *t*-values were positive, indicating that activation in discriminative ROIs is generally higher in TRs than in children with DD (Table 3). Furthermore, the magnitude of the *t*-values for threshold CM contrasts (i.e., CML6-*vs*-B and CML15-*vs*-B) and the M-*vs*-B contrast showed on average larger differences between the two groups compared to the other contrasts (Table 3). Interestingly, the ROIs with the largest differences between the two groups show higher contrast weights also in the multivariate analysis (Table 2).

Table 2. List of the ROIs with the highest performance.

	Hemisphere	ROI †	ROI-Region †	ROI Weight	Contrast Weight				
					M-*vs*-B	**P-*vs*-B**	**CML6-*vs*-B**	**CML15-*vs*-B**	**CML40-*vs*-B**
1	Right	Lateral Area 7P	Superior Parietal Cortex	1.000	−0.381	−0.277	−0.583	−0.525	−0.404
2	Left	Area PGp	Inferior Parietal Cortex	0.704	−0.405	−0.298	−0.613	−0.491	−0.361
3	Left	Area V6A	Dorsal Stream Visual Cortex	0.644	−0.407	−0.066	−0.549	−0.693	−0.220
4	Right	Medial Area 7A	Superior Parietal Cortex	0.633	−0.209	−0.257	−0.759	−0.458	−0.324
5	Left	Ventro-Medial Visual Area 1	Ventral Stream Visual Cortex	0.585	−0.112	0.119	−0.524	−0.664	−0.507
6	Left	Area Lateral Occipital 2	MT+ Complex and Neighboring Visual Area	0.539	−0.388	0.157	−0.495	−0.483	−0.589
7	Right	Area IFJ posterior	Inferior Frontal Cortex	0.521	−0.685	−0.477	−0.500	−0.230	−0.033
8	Right	Ventro-Medial Visual Area 1	Ventral Stream Visual Cortex	0.436	−0.546	−0.243	−0.436	−0.497	−0.454
9	Right	Area 5-L	Paracentral Lobular and Mid-Cingulate Cortex	0.315	−0.060	−0.077	−0.773	−0.524	−0.344
10	Right	Area PH	MT+ complex—Ventral stream fusiform face complex	0.290	−0.561	−0.573	−0.321	−0.424	−0.272
11	Right	Ventro-Medial Visual Area 2	Ventral Stream Visual Cortex	0.222	−0.655	−0.369	−0.396	−0.409	−0.333

† As parceled out in the HCP-MMP1 atlas [129]; M-*vs*-B: M stimulus vs. Baseline; P-*vs*-B: P stimulus vs. Baseline; CML6-*vs*-B: Coherent Motion Level 6% vs. Baseline; CML15-*vs*-B: Coherent Motion Level 15% vs. Baseline; CML40-*vs*-B: Coherent Motion Level 40% vs. Baseline.

Table 3. Group differences (*t*-tests) within each contrast map in the highest performance ROIs.

	Hemisphere	ROI †	ROI-Region †	M-*vs*-B	P-*vs*-B	CML6-*vs*-B	CML15-*vs*-B	CML40-*vs*-B
1	Right	Lateral Area 7P	Superior Parietal Cortex	2.309 (0.026)	1.713 (0.094)	3.662 (0.001)	2.993 (0.005)	2.009 (0.051)
2	Left	Area PGp	Inferior Parietal Cortex	2.023 (0.049)	1.770 (0.084)	2.985 (0.005)	2.503 (0.016)	1.579 (0.122)
3	Left	Area V6A	Dorsal Stream Visual Cortex	1.324 (0.193)	0.262 (0.795)	2.230 (0.031)	2.342 (0.024)	0.866 (0.391)
4	Right	Medial Area 7A	Superior Parietal Cortex	1.131 (0.264)	1.327 (0.192)	4.497 (<0.001)	2.413 (0.020)	1.916 (0.062)
5	Left	Ventro-Medial Visual Area 1	Ventral Stream Visual Cortex	0.839 (0.406)	−0.751 (0.457)	2.481 (0.017)	2.906 (0.006)	2.289 (0.027)
6	Left	Area Lateral Occipital 2	MT+ Complex and Neighboring Visual Area	1.805 (0.078)	−0.615 (0.542)	2.151 (0.037)	2.026 (0.049)	2.727 (0.009)
7	Right	Area IFJ posterior	Inferior Frontal Cortex	3.948 (<0.001)	2.468 (0.018)	2.698 (0.010)	1.430 (0.160)	0.194 (0.847)
8	Right	Ventro-Medial Visual Area 1	Ventral Stream Visual Cortex	3.014 (0.004)	1.288 (0.205)	1.845 (0.072)	1.905 (0.064)	1.810 (0.077)
9	Right	Area 5-L	Paracentral Lobular and Mid-Cingulate Cortex	0.312 (0.756)	0.316 (0.754)	4.441 (<0.001)	2.509 (0.016)	1.642 (0.108)
10	Right	Area PH	MT+ complex—Ventral stream fusiform face complex	3.538 (0.001)	3.078 (0.004)	1.553 (0.128)	2.110 (0.041)	1.401 (0.169)
11	Right	Ventro-Medial Visual Area 2	Ventral Stream Visual Cortex	2.628 (0.012)	1.437 (0.158)	1.467 (0.150)	1.789 (0.081)	1.148 (0.257)

† As parceled out in the HCP-MMP1 atlas [129] M-*vs*-B: M stimulus vs. Baseline; P-*vs*-B: P stimulus vs. Baseline; CML6-*vs*-B: Coherent Motion Level 6% vs. Baseline; CML15-*vs*-B: Coherent Motion Level 15% vs. Baseline; CML40-*vs*-B: Coherent Motion Level 40% vs. Baseline. Uncorrected *p*-values are reported in parentheses. NOTE: none of the significant differences survived after correction for multiple comparisons. Positive *t*-values indicate higher activations in TR than in children with DD.

Several nominally significant correlations were found between individual differences in the mean activation of the contrast maps in the significant ROIs and reading, VWM and phonology (see Supplementary Table S2). However, after applying the Bonferroni correction for multiple testing (threshold to infer statistical significance of p-value = 0.0003; 11 ROIs for five contrast maps for three neuropsychological domains), only the correlations between the mean activation of CML6-*vs*-B within the right lateral area 7P and the right medial area 7A, and reading survived (r = 0.552, p-value = 0.0001, and r = 0.540, p-value = 0.0002, respectively) (Figure 3). Specifically, a mean hyperactivation in these ROIs correlated with better performance in reading skills.

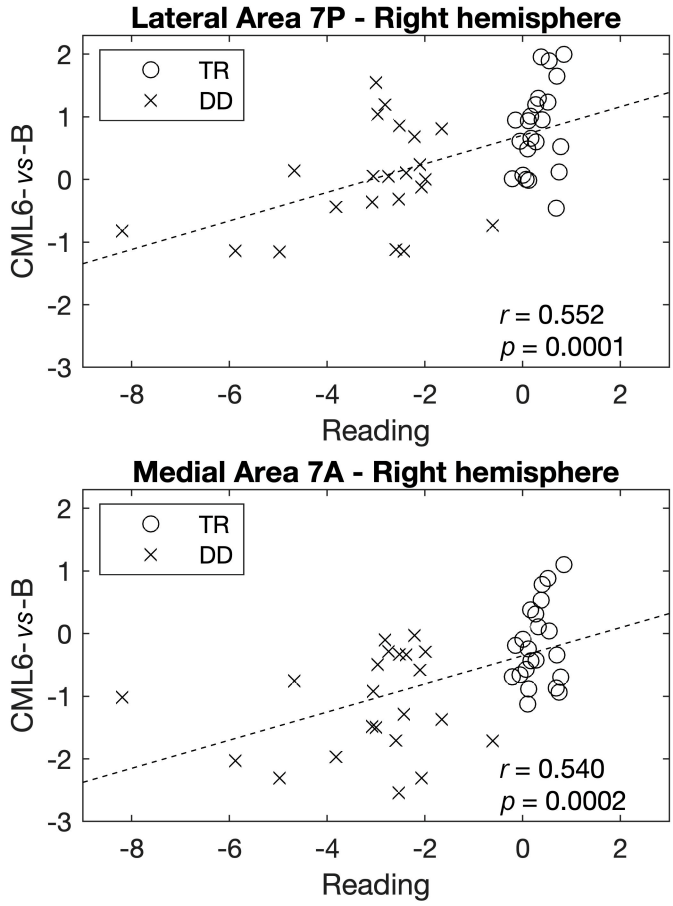

Figure 3. Bonferroni significant correlations between the mean activation of contrast maps within the significant ROIs and the neuropsychological domains in the total sample (n = 44). (**a**) Correlation between the mean activation of CML6-*vs*-B within the right lateral area 7P and reading. (**b**) Correlation between the mean activation of CML6-*vs*-B within the right medial area 7A and reading. Reading represents a mean score of text [98,99], single unrelated words and pronounceable pseudo-words [100,104] reading tests.

4. Discussion

To the best of our knowledge, the current study is the first to present an MKL-based methodology to differentiate groups of children with DD and age-matched TRs by using two visual tasks, one at both threshold and suprathreshold levels (sensitivity to motion coherence at 6%, 15% and 40%) and one in which more than one functional feature is simultaneously manipulated (full-field sinusoidal gratings controlled for both spatial and temporal frequencies and luminance contrast close to threshold levels). The multivariate approach performed by using the MKL-ROI classifier allows us to explore the widespread effects of the diagnosis of DD across multiple brain ROIs. Thus, it is more suitable to investigate the neural correlates of neurodevelopmental disorders involving wide brain

networks compared to univariate analysis, aimed to test the relationship between the diagnosis of DD and every single ROI.

Overall, the multivariate approach significantly discriminated between TRs and children with DD. In particular, we demonstrated that functional activation in the entire visual dorsal stream and the VAN ranks highest (Table 2). Although none of the T-test would survive the multiple comparison correction, their qualitative analysis indicated that activation in discriminative ROIs is generally higher in TRs than in children with DD (Table 3) [44,58,65–67]. This pattern of results is consistent with the notions that the fronto-parietal network is linked to "dorsal stream vulnerability" underlying several neurodevelopmental disorders and that the functionality of the M pathway is intimately related to the attention systems involved in attention control [51,52]. Deficits in the M pathway could influence higher visual processing stages through the dorsal stream and, therefore, lead to reading difficulties through impaired attentional orienting [32,38,69]. While the right fronto-parietal system is a crucial component of the network subserving the automatic shifting of attention [15,16], the left fronto-parietal system has been linked to auditory word form processing [135]. Developmental changes in the activation of the right fronto-parietal system have been linked to reading skills in both children with DD [136–138] and TRs [139]. Taken together, our findings suggest that a weakened or abnormal M input in the dorsal visual stream, and consequent dysfunction of the main fronto-parietal attentional network, are associated with SAS in DD [53,54].

Among the contrasts that influenced the classification algorithm most, functional activations induced by CM have a higher weight in the MKL classifier (Table 2). Although the contrast weights across the different levels of coherence are comparable within these ROIs, comparison among the coherence levels could be relevant to discriminate between TRs and children with DD. Consistently, the qualitative interpretation of the contrast T-values for CM at threshold levels (i.e., 6% and 15%) suggested that they are often higher in magnitude compared to the contrast weights for CM at suprathreshold level (i.e., 40%) (Table 3). The CML6 and CML15 showed the most group-discriminating activations in extra-visual areas lying within the dorsal portion of the M stream, the VAN and the salient network (Table 2) [15]. According to findings reported by independent psychophysical studies [93,94,125,126,140], we can hypothesize that the CML6 and CML15 represent relevant sensory stimuli requiring additional attentional resources to appropriately process the visual stimulus. According to this view, low CM levels might work as a 'circuit breaker' for the top-down attentional network, and they might imply the override of the current attentional set—usually activated by a high CM level—leading to the engagement of the frontal areas to enhance the attentional resources.

After a qualitative interpretation of the data, it is important to note that although children with DD showed lower activation compared to TRs for both the CML6-*vs*-B and the CML15-*vs*-B contrast maps, the magnitude of T for the CML6-*vs*-B is greater than those for the CML15-*vs*-B. Moreover, the mean activation of the CML6-*vs*-B within some areas of the right superior parietal cortex (i.e., the lateral area 7P and the medial area 7A) significantly correlated with reading (Supplementary Table S2). These findings are consistent with the SAS hypothesis [32] and the "perceptual noise exclusion deficit" [126,140]. Before the letter-to-sound mapping mechanism is applied, irrelevant lateral letters should be filtered out by accurate and rapid shifts in spatial and temporal visual attention [141–148]. This process may be more difficult if visual processing is hampered by deficits in attentional shifting and noise exclusion. Thus, the role of an auditory and phonological disorder aside, visual attention shifting and noise exclusion play a critical role in letter-to-speech sound integration during letter string processing because they are crucially involved in forming representations enabling efficient recognition of letters and letter sequences, identification of word shape and boundaries between words, representation of the sequential orthographic structure and the development of phonological representations [38,126,140].

Regarding the full-field sinusoidal gratings, the ROIs that lead the classification in this task have the lowest ROI weights in the MKL classifier (Table 2). Although the

M-*vs*-B and P-*vs*-B contrast weights are comparable within these ROIs, the M-*vs*-B T-values are often higher in magnitude compared to the P-*vs*-B (Table 3). So, as has been hypothesized for the CM, it is likely that the comparison between M and P stimuli could be relevant to the classification of TRs and children with DD. These findings further suggest that the M pathway is impaired in individuals with DD, whereas the other major parallel pathway of the visual system, the parvocellular stream, is less severely or not at all affected [38,39,54,69].

Limitations of the present investigation must be acknowledged. First, although we tested a larger sample size than those described in previous studies, the sample size of our study is still relatively small, which may have affected the classification performance and model generalizability [149]. Nonetheless, our sample was sufficient for a ranking profile of brain regions consistent with previous neuroimaging findings and etiological models of DD. It is plausible to predict that the greater power afforded by using larger samples would produce classification accuracy indices larger than those reported herein. Second, our results cannot be generalized to the general population since our aim was to use the MKL-based methodology as an alternative and stronger approach to investigate the role of the M pathway in DD and not to foster the diagnostic process. Third, the implemented procedure selects the minimal number of ROIs that provide a significant contribution to the classification. Consequently, ROIs that give a minor contribution to the classification but are involved in the "reading network" may not be highlighted.

5. Conclusions

The MKL-ROI approach used in the present study identified a highly discriminative network in the entire visual dorsal stream and the VAN when comparing children with DD and age-matched TRs. These brain areas lie within the fronto-parietal network, which is linked to the "dorsal stream vulnerability" underlying several neurodevelopmental disorders, and are known to be involved in deficits in the SAS in DD. Moreover, the implementation of both threshold- and suprathreshold-level visual stimuli in which more than one functional feature is simultaneously manipulated allowed us to better characterize the "dorsal stream vulnerability" underlying DD. According to the M theory of DD [38,54,69], a weakened or abnormal M input in the dorsal visual stream may lead to dysfunction of the main fronto-parietal attentional network [53,54] and difficulties in noise exclusion [150]. Our results further support the M visual pathway as a reliable biomarker of DD [39,151], which could lead to new approaches in the diagnosis of this neurodevelopmental disorder [152]. Moreover, these findings pave the way for the creation of early identification protocols, more effective prevention programs and better-defined rehabilitative treatments. Based on previous findings [35,47,153], it is plausible to assume that treatment programs based on M stream training could be a new approach for remedying and even preventing DD.

Supplementary Materials: The following are available online at https://www.mdpi.com/article/10.3390/brainsci11060722/s1. Figure S1. fMRI data processing flowchart. Data are represented with parallelepipedons, while operations on data are reported in rectangles. Figure S2. Multivariate analysis procedure flowchart. Data are represented with parallelepipedons, operations on data are reported in rectangles, dataset splits are reported in rhombuses. Dashed line rectangles cover all blocks included in the cross-validation procedures. Table S1. Bivariate correlations within reading (Table S1a) and within VWM (Table S1b) in the total sample. Table S2. Correlations between the mean activation of each contrast map within each significant ROIs and the neuropsychological domains in the total sample.

Author Contributions: Conceptualization, S.M., D.P. and F.A.; Data curation, S.M., V.T., C.A. and D.P.; Funding acquisition, S.M., D.P. and F.A.; Methodology, D.P., S.M., M.V., T.C. and F.A.; Writing—original draft, S.M., M.V. and D.P.; Writing—review & editing, C.A., T.C., V.T., C.M. and F.A. All authors have read and agreed to the published version of the manuscript.

Funding: This study was supported by Italian Ministry of Health Grants (Ricerca Corrente 2020 and Ricerca Corrente 2021 to Sara Mascheretti, and "Cinque per mille" and Ricerca Corrente 2021 to Denis Peruzzo).

Institutional Review Board Statement: The study was conducted according to the guidelines of the Declaration of Helsinki, and approved by the Ethics Committee of the Scientific Institute, IRCCS Eugenio Medea (protocol code 48/18-CE and date of approval 23 March 2018).

Informed Consent Statement: Informed consent was obtained from all subjects involved in the study.

Acknowledgments: The authors thank all the parents and children who took part in this study. They express their gratitude to Giancarlo Lembo, Luca Brenz, Lucia Vitari and Stefania Rizzello for helping with data collection. We gratefully acknowledge Andrea Facoetti for critically commenting on the article and providing useful insights. We thank Courtney K. Greenlaw for the English text revision. We gratefully acknowledge the support of NVIDIA Corporation for the computational resources used in this projects.

Conflicts of Interest: The authors declare no conflict of interest. (IRB:CE150166).

References

1. American Psychiatric Association. *DSM-V Manuale Diagnostico e Statistico dei Disturbi Mentali*, 5th ed.; American Psychiatric Press: Washington, DC, USA, 2013.
2. Peterson, R.L.; Pennington, B.F. Developmental Dyslexia. *Annu. Rev. Clin. Psychol.* **2015**, *11*, 283–307. [CrossRef]
3. Lyon, G.R.; Shaywitz, S.E.; Shaywitz, B.A. A definition of dyslexia. *Ann. Dyslexia* **2003**, *53*, 1–14. [CrossRef]
4. Bailey, S.K.; Aboud, K.S.; Nguyen, T.Q.; Cutting, L.E. Applying a network framework to the neurobiology of reading and dyslexia. *J. Neurodev. Disord.* **2018**, *10*, 37. [CrossRef]
5. Norton, E.S.; Wolf, M. Rapid Automatized Naming (RAN) and Reading Fluency: Implications for Understanding and Treatment of Reading Disabilities. *Annu. Rev. Psychol.* **2012**, *63*, 427–452. [CrossRef]
6. Wylie, J.; Thomson, J.; Leppänen, P.H.; Ackerman, R.; Kanniainen, L.; Prieler, T. Chapter 3. Cognitive processes and digital reading. In *Studies in Written Language and Literacy*; John Benjamins Publishing Company: Amsterdam, The Netherlands, 2018; Volume 17, pp. 57–90.
7. D'Mello, A.M.; Gabrieli, J.D.E. Cognitive Neuroscience of Dyslexia. *Lang. Speech Hear. Serv. Sch.* **2018**, *49*, 798–809. [CrossRef] [PubMed]
8. Vellutino, F.R.; Fletcher, J.M.; Snowling, M.J.; Scanlon, D.M. Specific reading disability (dyslexia): What have we learned in the past four decades? *J. Child Psychol. Psychiatry* **2004**, *45*, 2–40. [CrossRef] [PubMed]
9. Peterson, R.L.; Pennington, B.F. Developmental dyslexia. *Lancet* **2012**, *379*, 1997–2007. [CrossRef]
10. Pugh, K.R.; Mencl, W.E.; Jenner, A.R.; Katz, L.; Frost, S.J.; Lee, J.R.; Shaywitz, B.A. Functional neuroimaging studies of reading and reading disability (developmental dyslexia). *Ment. Retard. Dev. Disabil. Res. Rev.* **2000**, *6*, 207–213. [CrossRef]
11. Norton, E.S.; Beach, S.D.; DE Gabrieli, J. Neurobiology of dyslexia. *Curr. Opin. Neurobiol.* **2015**, *30*, 73–78. [CrossRef] [PubMed]
12. Nicolson, R.I.; Fawcett, A.J. Developmental dyslexia, learning and the cerebellum. *J. Neural Trasm Suppl.* **2005**, *69*, 19–36. [CrossRef]
13. Pugh, K.R.; Landi, N.; Preston, J.L.; Mencl, W.E.; Austin, A.C.; Sibley, D.; Fulbright, R.K.; Seidenberg, M.S.; Grigorenko, E.L.; Constable, R.T.; et al. The relationship between phonological and auditory processing and brain organization in beginning readers. *Brain Lang.* **2013**, *125*, 173–183. [CrossRef]
14. Ullman, M.T.; Earle, F.S.; Walenski, M.; Janacsek, K. The Neurocognition of Developmental Disorders of Language. *Annu. Rev. Psychol.* **2020**, *71*, 389–417. [CrossRef] [PubMed]
15. Corbetta, M.; Shulman, G.L. Control of goal-directed and stimulus-driven attention in the brain. *Nat. Rev. Neurosci.* **2002**, *3*, 201–215. [CrossRef]
16. Corbetta, M.; Shulman, G.L. Spatial Neglect and Attention Networks. *Annu. Rev. Neurosci.* **2011**, *34*, 569–599. [CrossRef] [PubMed]
17. McCandliss, B.D.; Cohen, L.; Dehaene, S. The visual word form area: Expertise for reading in the fusiform gyrus. *Trends Cogn. Sci.* **2003**, *7*, 293–299. [CrossRef]
18. Pennington, B.F. From single to multiple deficit models of developmental disorders. *Cognition* **2006**, *101*, 385–413. [CrossRef]
19. Castles, A.; Coltheart, M. Is there a causal link from phonological awareness to success in learning to read? *Cognition* **2004**, *91*, 77–111. [CrossRef]
20. Tallal, P. Auditory temporal perception, phonics, and reading disabilities in children. *Brain Lang.* **1980**, *9*, 182–198. [CrossRef]
21. McAnally, K.I.; Stein, J.F. Auditory temporal coding in dyslexia. *Proc. Biol. Sci.* **1996**, *263*, 961–965.
22. Hämäläinen, J.A.; Guttorm, T.K.; Richardson, U.; Alku, P.; Lyytinen, H.; Leppänen, P.H.T. Auditory Event-Related Potentials Measured in Kindergarten Predict Later Reading Problems at School Age. *Dev. Neuropsychol.* **2013**, *38*, 550–566. [CrossRef]
23. Hornickel, J.; Kraus, N. Unstable Representation of Sound: A Biological Marker of Dyslexia. *J. Neurosci.* **2013**, *33*, 3500–3504. [CrossRef]

24. Vandermosten, M.; Boets, B.; Luts, H.; Poelmans, H.; Golestani, N.; Wouters, J.; Ghesquiere, P. Adults with dyslexia are impaired in categorizing speech and nonspeech sounds on the basis of temporal cues. *Proc. Natl. Acad. Sci. USA* **2010**, *107*, 10389–10394. [CrossRef]
25. Vandermosten, M.; Boets, B.; Luts, H.; Poelmans, H.; Wouters, J.; Ghesquière, P. Impairments in speech and nonspeech sound categorization in children with dyslexia are driven by temporal processing difficulties. *Res. Dev. Disabil.* **2011**, *32*, 593–603. [CrossRef]
26. Molfese, D.L. Predicting Dyslexia at 8 Years of Age Using Neonatal Brain Responses. *Brain Lang.* **2000**, *72*, 238–245. [CrossRef] [PubMed]
27. Leppänen, P.H.; Hamalainen, J.; Salminen, H.K.; Eklund, K.M.; Guttorm, T.K.; Lohvansuu, K.; Puolakanaho, A.; Lyytinen, H. Newborn brain event-related potentials revealing atypical processing of sound frequency and the subsequent association with later literacy skills in children with familial dyslexia. *Cortex* **2010**, *46*, 1362–1376. [CrossRef] [PubMed]
28. Van Der Leij, A.; Van Bergen, E.; Van Zuijen, T.L.; De Jong, P.; Maurits, N.; Maassen, B.A.M. Precursors of Developmental Dyslexia: An Overview of the Longitudinal Dutch Dyslexia Programme Study. *Dyslexia* **2013**, *19*, 191–213. [CrossRef] [PubMed]
29. Cantiani, C.; Riva, V.; Piazza, C.; Bettoni, R.; Molteni, M.; Choudhury, N.; Marino, C.; Benasich, A.A. Auditory discrimination predicts linguistic outcome in Italian infants with and without familial risk for language learning impairment. *Dev. Cogn. Neurosci.* **2016**, *20*, 23–34. [CrossRef] [PubMed]
30. Clark, K.A.; Helland, T.; Specht, K.; Narr, K.L.; Manis, F.R.; Toga, A.W.; Hugdahl, K. Neuroanatomical precursors of dyslexia identified from pre-reading through to age 11. *Brain* **2014**, *137*, 3136–3141. [CrossRef]
31. Lervåg, A.; Hulme, C. Rapid Automatized Naming (RAN) Taps a Mechanism That Places Constraints on the Development of Early Reading Fluency. *Psychol. Sci.* **2009**, *20*, 1040–1048. [CrossRef]
32. Hari, R.; Renvall, H. Impaired processing of rapid stimulus sequences in dyslexia. *Trends Cogn. Sci.* **2001**, *5*, 525–532. [CrossRef]
33. Renvall, H.; Hari, R. Auditory Cortical Responses to Speech-Like Stimuli in Dyslexic Adults. *J. Cogn. Neurosci.* **2002**, *14*, 757–768. [CrossRef]
34. Franceschini, S.; Gori, S.; Ruffino, M.; Pedrolli, K.; Facoetti, A. A Causal Link between Visual Spatial Attention and Reading Acquisition. *Curr. Biol.* **2012**, *22*, 814–819. [CrossRef] [PubMed]
35. Franceschini, S.; Gori, S.; Ruffino, M.; Viola, S.; Molteni, M.; Facoetti, A. Action Video Games Make Dyslexic Children Read Better. *Curr. Biol.* **2013**, *23*, 462–466. [CrossRef] [PubMed]
36. Lallier, M.; Donnadieu, S.; Valdois, S. Investigating the role of visual and auditory search in reading and developmental dyslexia. *Front. Hum. Neurosci.* **2013**, *7*, 597. [CrossRef]
37. Plaza, M.; Cohen, H. The contribution of phonological awareness and visual attention in early reading and spelling. *Dyslexia* **2006**, *13*, 67–76. [CrossRef]
38. Vidyasagar, T.R.; Pammer, K. Dyslexia: A deficit in visuo-spatial attention, not in phonological processing. *Trends Cogn. Sci.* **2010**, *14*, 57–63. [CrossRef]
39. Stein, J. The current status of the magnocellular theory of developmental dyslexia. *Neuropsychology* **2019**, *130*, 66–77. [CrossRef] [PubMed]
40. Cohen, L.; Dehaene, S.; Vinckier, F.; Jobert, A.; Montavont, A. Reading normal and degraded words: Contribution of the dorsal and ventral visual pathways. *NeuroImage* **2008**, *40*, 353–366. [CrossRef] [PubMed]
41. Liu, C.-S.J.; Bryan, R.N.; Miki, A.; Woo, J.H.; Liu, G.T.; Elliott, M.A. Magnocellular and parvocellular visual pathways have different blood oxygen level-dependent signal time courses in human primary visual cortex. *Am. J. Neuroradiol.* **2006**, *27*, 1628–1634. [PubMed]
42. Zhang, P.; Zhou, H.; Wen, W.; He, S. Layer-specific response properties of the human lateral geniculate nucleus and superior colliculus. *NeuroImage* **2015**, *111*, 159–166. [CrossRef]
43. Denison, R.N.; Vu, A.T.; Yacoub, E.; Feinberg, D.A.; Silver, M.A. Functional mapping of the magnocellular and parvocellular subdivisions of human LGN. *NeuroImage* **2014**, *102*, 358–369. [CrossRef]
44. Eden, G.F.; VanMeter, J.W.; Rumsey, J.M.; Maisog, J.M.; Woods, R.P.; Zeffiro, T.A. Abnormal processing of visual motion in dyslexia revealed by functional brain imaging. *Nature* **1996**, *382*, 66–69. [CrossRef]
45. Rizzolatti, G.; Matelli, M. Two different streams form the dorsal visual system: Anatomy and functions. *Exp. Brain Res.* **2003**, *153*, 146–157. [CrossRef]
46. Galletti, C.; Gamberini, M.; Kutz, D.F.; Fattori, P.; Luppino, G.; Matelli, M. The cortical connections of area V6: An occipito-parietal network processing visual information. *Eur. J. Neurosci.* **2001**, *13*, 1572–1588. [CrossRef]
47. Gori, S.; Facoetti, A. Perceptual learning as a possible new approach for remediation and prevention of developmental dyslexia. *Vis. Res.* **2014**, *99*, 78–87. [CrossRef]
48. Galletti, C.; Fattori, P. The dorsal visual stream revisited: Stable circuits or dynamic pathways? *Cortex* **2018**, *98*, 203–217. [CrossRef]
49. Pammer, K.; Hansen, P.; Holliday, I.; Cornelissen, P. Attentional shifting and the role of the dorsal pathway in visual word recognition. *Neuropsychology* **2006**, *44*, 2926–2936. [CrossRef]
50. Vidyasagar, T.R. Reading into neuronal oscillations in the visual system: Implications for developmental dyslexia. *Front. Hum. Neurosci.* **2013**, *7*, 811. [CrossRef] [PubMed]
51. Braddick, O.; Atkinson, J. Development of human visual function. *Vis. Res.* **2011**, *51*, 1588–1609. [CrossRef] [PubMed]

52. Atkinson, J. The Davida Teller Award lecture, 2016: Visual Brain development: A review of dorsal stream vulnerability-motion, mathematics, amblyopia, actions, and attention. *J. Vis.* **2017**, *17*, 26. [CrossRef] [PubMed]
53. Livingstone, M.S.; Rosen, G.D.; Drislane, F.W.; Galaburda, A.M. Physiological and anatomical evidence for a magnocellular defect in developmental dyslexia. *Proc. Natl. Acad. Sci. USA* **1991**, *88*, 7943–7947. [CrossRef] [PubMed]
54. Stein, J.; Walsh, V. To see but not to read; the magnocellular theory of dyslexia. *Trends Neurosci.* **1997**, *20*, 147–152. [CrossRef]
55. Vidyasagar, T.R. Gating of neuronal responses in macaque primary visual cortex by an attentional spotlight. *NeuroReport* **1998**, *9*, 1947–1952. [CrossRef]
56. Stein, J. Dyslexia: The Role of Vision and Visual Attention. *Curr. Dev. Disord. Rep.* **2014**, *1*, 267–280. [CrossRef] [PubMed]
57. Antal, A.; Baudewig, J.; Paulus, W.; Dechent, P. The posterior cingulate cortex and planum temporale/parietal operculum are activated by coherent visual motion. *Vis. Neurosci.* **2008**, *25*, 17–26. [CrossRef] [PubMed]
58. Heim, S.; Grande, M.; Pape-Neumann, J.; van Ermingen, M.; Meffert, E.; Grabowska, A.; Huber, W.; Amunts, K. Interaction of phonological awareness and 'magnocellular' processing during normal and dyslexic reading: Behavioural and fMRI investigations. *Dyslexia* **2010**, *16*, 258–282. [CrossRef] [PubMed]
59. Heim, S.; Weidner, R.; Von Overheidt, A.-C.; Tholen, N.; Grande, M.; Amunts, K. Experimental induction of reading difficulties in normal readers provides novel insights into the neurofunctional mechanisms of visual word recognition. *Brain Struct. Funct.* **2013**, *219*, 461–471. [CrossRef]
60. Costagli, M.; Ueno, K.; Sun, P.; Gardner, J.L.; Wan, X.; Ricciardi, E.; Pietrini, P.; Tanaka, K.; Cheng, K. Functional Signalers of Changes in Visual Stimuli: Cortical Responses to Increments and Decrements in Motion Coherence. *Cereb. Cortex* **2012**, *24*, 110–118. [CrossRef]
61. Csete, G.; Szabó, N.; Rokszin, A.; Tóth, E.; Braunitzer, G.; Benedek, G.; Vécsei, L.; Kincses, Z.T. An investigation of the white matter microstructure in motion detection using diffusion MRI. *Brain Res.* **2014**, *1570*, 35–42. [CrossRef]
62. Danelli, L.; Berlingeri, M.; Bottini, G.; Ferri, F.; Vacchi, L.; Sberna, M.; Paulesu, E. Neural intersections of the phonological, visual magnocellular and motor/cerebellar systems in normal readers: Implications for imaging studies on dyslexia. *Hum. Brain Mapp.* **2012**, *34*, 2669–2687. [CrossRef] [PubMed]
63. Qian, Y.; Deng, Y.; Zhao, J.; Bi, H.-Y. Magnocellular-dorsal pathway function is associated with orthographic but not phonological skill: fMRI evidence from skilled Chinese readers. *Neuropsychology* **2015**, *71*, 84–90. [CrossRef] [PubMed]
64. Singh, K.; Smith, A.T.; Greenlee, M. Spatiotemporal Frequency and Direction Sensitivities of Human Visual Areas Measured Using fMRI. *NeuroImage* **2000**, *12*, 550–564. [CrossRef] [PubMed]
65. Demb, J.B.; Boynton, G.M.; Best, M.; Heeger, D.J. Psychophysical evidence for a magnocellular pathway deficit in dyslexia. *Vis. Res.* **1998**, *38*, 1555–1559. [CrossRef]
66. Demb, J.; Boynton, G.M.; Heeger, D.J. Brain activity in visual cortex predicts individual differences in reading performance. *Proc. Natl. Acad. Sci. USA* **1997**, *94*, 13363–13366. [CrossRef]
67. Olulade, O.A.; Napoliello, E.M.; Eden, G.F. Abnormal Visual Motion Processing Is Not a Cause of Dyslexia. *Neuron* **2013**, *79*, 180–190. [CrossRef]
68. Ferrera, V.P.; Nealey, T.A.; Maunsell, J.H.R. Mixed parvocellular and magnocellular geniculate signals in visual area V4. *Nat. Cell Biol.* **1992**, *358*, 756–758. [CrossRef]
69. Boden, C.; Giaschi, D. M-stream deficits and reading-related visual processes in developmental dyslexia. *Psychol. Bull.* **2007**, *133*, 346–366. [CrossRef]
70. Giraldo-Chica, M.; Schneider, K.A. Hemispheric asymmetries in the orientation and location of the lateral geniculate nucleus in dyslexia. *Dyslexia* **2018**, *24*, 197–203. [CrossRef]
71. Giraldo-Chica, M.; Hegarty, J.P.; Schneider, K.A. Morphological differences in the lateral geniculate nucleus associated with dyslexia. *NeuroImage Clin.* **2015**, *7*, 830–836. [CrossRef] [PubMed]
72. Lovegrove, W.; Martin, F.; Bowling, A.; Blackwood, M.; Badcock, D.; Paxton, S. Contrast sensitivity functions and specific reading disability. *Neuropsychology* **1982**, *20*, 309–315. [CrossRef]
73. Martin, F.; Lovegrove, W. The effects of field size and luminance on contrast sensitivity differences between specifically reading disabled and normal children. *Neuropsychology* **1984**, *22*, 73–77. [CrossRef]
74. Martin, F.; Lovegrove, W. Flicker Contrast Sensitivity in Normal and Specifically Disabled Readers. *Perception* **1987**, *16*, 215–221. [CrossRef] [PubMed]
75. Evans, B.J.; Drasdo, N.; Richards, I.L. An investigation of some sensory and refractive visual factors in dyslexia. *Vis. Res.* **1994**, *34*, 1913–1926. [CrossRef]
76. Cornelissen, P.; Richardson, A.; Mason, A.; Fowler, S.; Stein, J. Contrast sensitivity and coherent motion detection measured at photopic luminance levels in dyslexics and controls. *Vis. Res.* **1995**, *35*, 1483–1494. [CrossRef]
77. Borsting, E.; Ridder, W.H.; Dudeck, K.; Kelley, C.; Matsui, L.; Motoyama, J. The presence of a magnocellular defect depends on the type of dyslexia. *Vis. Res.* **1996**, *36*, 1047–1053. [CrossRef]
78. Hansen, P.C.; Stein, J.F.; Orde, S.R.; Winter, J.L.; Talcott, J.B. Are dyslexics??? visual deficits limited to measures of dorsal stream function? *NeuroReport* **2001**, *12*, 1527–1530. [CrossRef]
79. Meng, X.; Cheng-Lai, A.; Zeng, B.; Stein, J.F.; Zhou, X. Dynamic visual perception and reading development in Chinese school children. *Ann. Dyslexia* **2011**, *61*, 161–176. [CrossRef]

80. Talcott, J.B.; Gram, A.; Van Ingelghem, M.; Witton, C.; Stein, J.F.; Toennessen, F.E. Impaired sensitivity to dynamic stimuli in poor readers of a regular orthography. *Brain Lang.* **2003**, *87*, 259–266. [CrossRef]
81. Talcott, J.B.; Hansen, P.C.; Assoku, E.L.; Stein, J.F. Visual motion sensitivity in dyslexia: Evidence for temporal and energy integration deficits. *Neuropsychology* **2000**, *38*, 935–943. [CrossRef]
82. Witton, C.; Talcott, J.; Hansen, P.; Richardson, A.; Griffiths, T.; Rees, A.; Stein, J.; Green, G. Sensitivity to dynamic auditory and visual stimuli predicts nonword reading ability in both dyslexic and normal readers. *Curr. Biol.* **1998**, *8*, 791–797. [CrossRef]
83. Boets, B.; Vandermosten, M.; Cornelissen, P.; Wouters, J.; Ghesquière, P. Coherent Motion Sensitivity and Reading Development in the Transition From Prereading to Reading Stage. *Child Dev.* **2011**, *82*, 854–869. [CrossRef]
84. May, J.G.; Lovegrove, W.J.; Martin, F.; Nelson, P. Pattern-elicited visual evoked potentials in good and poor readers. *Clin. Vis. Sci.* **1991**, *6*, 131–136.
85. Lehmkuhle, S.; Garzia, R.P.; Turner, L.; Hash, T.; Baro, J.A. A Defective Visual Pathway in Children with Reading Disability. *N. Engl. J. Med.* **1993**, *328*, 989–996. [CrossRef]
86. Kubova, Z.; Kuba, M.; Peregrin, J.; Nováková, V. Visual evoked potential evidence for magnocellular system deficit in dyslexia. *Physiol. Res.* **1996**, *45*, 87–89.
87. Merigan, W.H.; Maunsell, J.H.R. How Parallel are the Primate Visual Pathways? *Annu. Rev. Neurosci.* **1993**, *16*, 369–402. [CrossRef] [PubMed]
88. Danelli, L.; Berlingeri, M.; Bottini, G.; Borghese, N.A.; Lucchese, M.; Sberna, M.; Price, C.J.; Paulesu, E. How many deficits in the same dyslexic brains? A behavioural and fMRI assessment of comorbidity in adult dyslexics. *Cortex* **2017**, *97*, 125–142. [CrossRef]
89. Taylor, C.; Olulade, O.; Luetje, M.; Eden, G. An fMRI study of coherent visual motion processing in children and adults. *NeuroImage* **2018**, *173*, 223–239. [CrossRef] [PubMed]
90. Laycock, R.; Crewther, S. Towards an understanding of the role of the 'magnocellular advantage' in fluent reading. *Neurosci. Biobehav. Rev.* **2008**, *32*, 1494–1506. [CrossRef]
91. Skottun, B.C. A few remarks on the utility of visual motion perception to assess the integrity of the magnocellular system or the dorsal stream. *Cortex* **2016**, *79*, 155–158. [CrossRef] [PubMed]
92. Peiker, I.; David, N.; Schneider, T.R.; Nolte, G.; Schöttle, D.; Engel, A.K. Perceptual Integration Deficits in Autism Spectrum Disorders Are Associated with Reduced Interhemispheric Gamma-Band Coherence. *J. Neurosci.* **2015**, *35*, 16352–16361. [CrossRef] [PubMed]
93. Robertson, C.E.; Thomas, C.; Kravitz, D.J.; Wallace, G.; Baron-Cohen, S.; Martin, A.; Baker, C.I. Global motion perception deficits in autism are reflected as early as primary visual cortex. *Brain* **2014**, *137*, 2588–2599. [CrossRef]
94. Buchel, C.; Josephs, O.; Rees, G.; Turner, R.; Frith, C.D.; Friston, K.J. The functional anatomy of attention to visual motion. A functional MRI study. *Brain* **1998**, *121*, 1281–1294. [CrossRef]
95. Cheng, K.; Fujita, H.; Kanno, I.; Miura, S.; Tanaka, K. Human cortical regions activated by wide-field visual motion: An H2(15)O PET study. *J. Neurophysiol.* **1995**, *74*, 413–427. [CrossRef] [PubMed]
96. Culham, J.C.; Brandt, S.A.; Cavanagh, P.; Kanwisher, N.G.; Dale, A.M.; Tootell, R.B.H. Cortical fMRI Activation Produced by Attentive Tracking of Moving Targets. *J. Neurophysiol.* **1998**, *80*, 2657–2670. [CrossRef]
97. Könönen, M.; Pääkkönen, A.; Pihlajamäki, M.; Partanen, K.; Karjalainen, P.A.; Soimakallio, S.; Aronen, H.J. Visual processing of coherent rotation in the central visual field: An fMRI study. *Perception* **2003**, *32*, 1247–1257. [CrossRef] [PubMed]
98. Van Schouwenburg, M.R.; Ouden, H.E.M.D.; Cools, R. The Human Basal Ganglia Modulate Frontal-Posterior Connectivity during Attention Shifting. *J. Neurosci.* **2010**, *30*, 9910–9918. [CrossRef]
99. Van Schouwenburg, M.R.; Ouden, H.E.M.D.; Cools, R. Selective Attentional Enhancement and Inhibition of Fronto-Posterior Connectivity by the Basal Ganglia during Attention Switching. *Cereb. Cortex* **2015**, *25*, 1527–1534. [CrossRef]
100. Patel, S.S.; Bedell, H.E.; Tsang, D.K.; Ukwade, M.T. Relationship between threshold and suprathreshold perception of position and stereoscopic depth. *J. Opt. Soc. Am. A* **2009**, *26*, 847–861. [CrossRef]
101. Fechner, G.T. *Elemente der Psychophysik [Elements of Psychophysics]*, 2nd ed.; Breitkopf und Härtel: Leipzig, Germany, 1860.
102. Green, D.M.; Swets, J.A. *Signal Detection Theory and Psychophysics*; A Reprint with Corrections of the Original 1966 ed.; Robert, E., Ed.; Krieger Publishing, Co: Huntington, NY, USA, 1974.
103. Peruzzo, D.; PICOS-Veneto Group; Castellani, U.; Perlini, C.; Bellani, M.; Marinelli, V.; Rambaldelli, G.; Lasalvia, A.; Tosato, S.; De Santi, K.; et al. Classification of first-episode psychosis: A multi-modal multi-feature approach integrating structural and diffusion imaging. *J. Neural Transm.* **2014**, *122*, 897–905. [CrossRef]
104. Riva, V.; Mozzi, A.; Forni, D.; Trezzi, V.; Giorda, R.; Riva, S.; Villa, M.; Sironi, M.; Cagliani, R.; Mascheretti, S. The influence of DCDC2 risk genetic variants on reading: Testing main and haplotypic effects. *Neuropsychology* **2019**, *130*, 52–58. [CrossRef] [PubMed]
105. American Psychiatric Association. *Diagnostic and Statistical Manual of Mental Disorders*, 4th ed.; American Psychiatric Association: Washington, DC, USA, 2006.
106. Riva, V.; Battaglia, M.; Nobile, M.; Cattaneo, F.; Lazazzera, C.; Mascheretti, S.; Giorda, R.; Mérette, C.; Émond, C.; Maziade, M.; et al. GRIN2B predicts attention problems among disadvantaged children. *Eur. Child Adolesc. Psychiatry* **2014**, *24*, 827–836. [CrossRef]
107. Wechsler, D. *Wechsler Intelligence Scale for Children*, 3rd ed.; Organizzazioni Speciali: Firenze, Italy, 2006.
108. Cornoldi, C. *Nuove Prove di Lettura MT per la Scuola Media Inferiore*; Organizzazioni Speciali: Firenze, Italy, 1995.
109. Cornoldi, C.; Colpo, G. *Prove di Lettura MT per la Scuola Elementare*, 2nd ed.; Organizzazioni Speciali: Firenze, Italy, 1998.

110. Sartori, G.; Job, R.; Tressoldi, P.E. *Batteria per la Valutazione Della Dislessia e Della Disortografia Evolutive*; Organizzazioni Speciali: Firenze, Italy, 1995.
111. Arina, S.; Iervolino, I.; Stella, G. Prima raccolta di dati normativi per la valutazione della dislessia evolutiva negli adolescenti su un campione di scuola secondaria di secondo grado. *Dislessia* **2013**, *10*, 9–38.
112. Reynolds, C.R.; Bigler, E.D. *Test of Memory and Learning*; Erickson: Trento, Italy, 1994.
113. Bertelli, B.; Bilancia, G. *VAUMeLF Batteria per la Valutazione Dell'attenzione Uditiva e Della Memoria di Lavoro Fonologica Nell'età Evolutiva*; Organizzazioni Speciali: Firenze, Italy, 2006.
114. Briggs, G.G.; Nebes, R.D. Patterns of Hand Preference in a Student Population. *Cortex* **1975**, *11*, 230–238. [CrossRef]
115. Conners, C.K. *Manual for Conners' Rating Scales*; Multi-Health Systems: North Tonawanda, NY, USA, 1989.
116. Conners, C.K.; Sitarenios, G.; Parker, J.D.A.; Epstein, J.N. The Revised Conners' Parent Rating Scale (CPRS-R): Factor Structure, Reliability, and Criterion Validity. *J. Abnorm. Child Psychol.* **1998**, *26*, 257–268. [CrossRef]
117. Nobile, M.; Alberti, B.; Zuddas, A. *CRS-R. Conners' Rating Scale—Revised*; Organizzazioni Speciali: Firenze, Italy, 2007.
118. Cunningham, A.E.; Stanovich, K.E. Early reading acquisition and its relation to reading experience and ability 10 years later. *Dev. Psychol.* **1997**, *33*, 934–945. [CrossRef]
119. Ferrer, E.; Shaywitz, B.A.; Holahan, J.M.; Marchione, K.; Shaywitz, S.E. Uncoupling of Reading and IQ Over Time. *Psychol. Sci.* **2009**, *21*, 93–101. [CrossRef] [PubMed]
120. Nagy, W.E.; Herman, P.A.; Anderson, R.C. Learning Words from Context. *Read. Res. Q.* **1985**, *20*, 233. [CrossRef]
121. Ramsden, S.; Richardson, F.M.; Josse, G.; Shakeshaft, C.; Seghier, M.L.; Price, C.J. The influence of reading ability on subsequent changes in verbal IQ in the teenage years. *Dev. Cogn. Neurosci.* **2013**, *6*, 30–39. [CrossRef] [PubMed]
122. Stanovich, K.E.; Cunningham, A.E. Where does knowledge come from? Specific associations between print exposure and information acquisition. *J. Educ. Psychol.* **1993**, *85*, 211–229. [CrossRef]
123. Swanborn, M.; De Glopper, K. Incidental Word Learning While Reading: A Meta-Analysis. *Rev. Educ. Res.* **1999**, *69*, 261–285. [CrossRef]
124. Hollingshead, A.B. *Four Factor Index of Social Status*; Yale University: New Haven, CT, USA, 1975.
125. Cicchini, G.M.; Marino, C.; Mascheretti, S.; Perani, D.; Morrone, M.C. Strong Motion Deficits in Dyslexia Associated with DCDC2 Gene Alteration. *J. Neurosci.* **2015**, *35*, 8059–8064. [CrossRef] [PubMed]
126. Sperling, A.J.; Lu, Z.-L.; Manis, F.R.; Seidenberg, M.S. Deficits in perceptual noise exclusion in developmental dyslexia. *Nat. Neurosci.* **2005**, *8*, 862–863. [CrossRef] [PubMed]
127. Tustison, N.J.; Avants, B.B.; Cook, P.A.; Zheng, Y.; Egan, A.; Yushkevich, P.A.; Gee, J.C. N4ITK: Improved N3 Bias Correction. *IEEE Trans. Med. Imaging* **2010**, *29*, 1310–1320. [CrossRef] [PubMed]
128. Glasser, M.F.; Coalson, T.S.; Robinson, E.C.; Hacker, C.D.; Harwell, J.; Yacoub, E.; Ugurbil, E.Y.K.; Andersson, J.; Beckmann, C.F.; Jenkinson, M.; et al. A multi-modal parcellation of human cerebral cortex. *Nat. Cell Biol.* **2016**, *536*, 171–178. [CrossRef]
129. Bach, F.R.; Lanckriet, G.R.G.; Jordan, M.I. Multiple kernel learning, conic duality, and the SMO algorithm. In Proceedings of the Twenty-first international conference on Machine learning—ICML '04, Association for Computing Machinery (ACM), New York, NY, USA, 4–8 July 2004; p. 6.
130. Lanckriet, G.R.G.; Cristianini, N.; Bartlett, P.; El Ghaoui, L.; Jordan, M.I. Learning the kernel matrix with semidefinite programming. *J. Mach. Learn. Res.* **2004**, *5*, 27–52.
131. Xu, Z.; Jin, R.; Yang, H.; King, I.; Lyu, M.R. Simple and efficient multiple kernel learning by group lasso. In Proceedings of the 27th International Conference on Machine Learning (ICML-10), Haifa, Israel, 21–24 June 2010.
132. Poldrack, R.A.; Huckins, G.; Varoquaux, G. Establishment of best practices for evidence for prediction, a review. *JAMA Psychiatry* **2019**, *77*, 534–540. [CrossRef]
133. Bellotti, T.; Nouretdinov, I.; Yang, M.; Gammerman, A. Feature selection. In *Balasubramanian, Conformal Prediction for Reliable Machine Learning: Theory, Adaptations and Applications*; Ho, V.N., Vovk, S.-S., Eds.; Morgan Kaufmann Publishers: Burlington, MA, USA, 2014; pp. 116–130.
134. Haufe, S.; Meinecke, F.; Görgen, K.; Dähne, S.; Haynes, J.-D.; Blankertz, B.; Bießmann, F. On the interpretation of weight vectors of linear models in multivariate neuroimaging. *NeuroImage* **2014**, *87*, 96–110. [CrossRef]
135. Price, C.; Winterburn, D.; Giraud, A.; Moore, C.; Noppeney, U. Cortical localisation of the visual and auditory word form areas: A reconsideration of the evidence. *Brain Lang.* **2003**, *86*, 272–286. [CrossRef]
136. Hoeft, F.; Hernandez, A.; McMillon, G.; Taylor-Hill, H.; Martindale, J.L.; Meyler, A.; Keller, T.A.; Siok, W.T.; Deutsch, G.K.; Just, M.; et al. Neural Basis of Dyslexia: A Comparison between Dyslexic and Nondyslexic Children Equated for Reading Ability. *J. Neurosci.* **2006**, *26*, 10700–10708. [CrossRef] [PubMed]
137. Hoeft, F.; McCandliss, B.D.; Black, J.M.; Gantman, A.; Zakerani, N.; Hulme, C.; Lyytinen, H.; Whitfield-Gabrieli, S.; Glover, G.H.; Reiss, A.L.; et al. Neural systems predicting long-term outcome in dyslexia. *Proc. Natl. Acad. Sci. USA* **2011**, *108*, 361–366. [CrossRef] [PubMed]
138. Flint, J.; Timpson, N.; Munafò, M. Assessing the utility of intermediate phenotypes for genetic mapping of psychiatric disease. *Trends Neurosci.* **2014**, *37*, 733–741. [CrossRef]
139. Turkeltaub, P.; Gareau, L.; Flowers, D.L.; Zeffiro, A.T.; Eden, G.F. Development of neural mechanisms for reading. *Nat. Neurosci.* **2003**, *6*, 767–773. [CrossRef]

140. Sperling, A.J.; Lu, Z.-L.; Manis, F.R.; Seidenberg, M.S. Motion-Perception Deficits and Reading Impairment. *Psychol. Sci.* **2006**, *17*, 1047–1053. [CrossRef] [PubMed]
141. Cestnick, L.; Coltheart, M. The relationship between language-processing and visual-processing deficits in developmental dyslexia. *Cognition* **1999**, *71*, 231–255. [CrossRef]
142. Facoetti, A.; Corradi, N.; Ruffino, M.; Gori, S.; Zorzi, M. Visual spatial attention and speech segmentation are both impaired in preschoolers at familial risk for developmental dyslexia. *Dyslexia* **2010**, *16*, 226–239. [CrossRef]
143. Facoetti, A.; Ruffino, M.; Peru, A.; Paganoni, P.; Chelazzi, L. Sluggish engagement and disengagement of non-spatial attention in dyslexic children. *Cortex* **2008**, *44*, 1221–1233. [CrossRef] [PubMed]
144. Facoetti, A.; Zorzi, M.; Cestnick, L.; Lorusso, M.L.; Molteni, M.; Paganoni, P.; Umiltà, C.; Mascetti, G.G. The relationship between visuo-spatial attention and nonword reading in developmental dyslexia. *Cogn. Neuropsychol.* **2006**, *23*, 841–855. [CrossRef]
145. Ruffino, M.; Trussardi, A.N.; Gori, S.; Finzi, A.; Giovagnoli, S.; Menghini, D.; Benassi, M.; Molteni, M.; Bolzani, R.; Vicari, S.; et al. Attentional engagement deficits in dyslexic children. *Neuropsychology* **2010**, *48*, 3793–3801. [CrossRef] [PubMed]
146. Franceschini, S.; Mascheretti, S.; Bertoni, S.; Trezzi, V.; Andreola, C.; Gori, S.; Facoetti, A. Sluggish dorsally-driven inhibition of return during orthographic processing in adults with dyslexia. *Brain Lang.* **2018**, *179*, 1–10. [CrossRef]
147. Fu, W.; Zhao, J.; Ding, Y.; Wang, Z. Dyslexic children are sluggish in disengaging spatial attention. *Dyslexia* **2019**, *25*, 158–172. [CrossRef]
148. Krause, M.B. Pay Attention!: Sluggish Multisensory Attentional Shifting as a Core Deficit in Developmental Dyslexia. *Dyslexia* **2015**, *21*, 285–303. [CrossRef]
149. Varoquaux, G. Cross-validation failure: Small sample sizes lead to large error bars. *NeuroImage* **2018**, *180*, 68–77. [CrossRef] [PubMed]
150. Conlon, E.G.; Lilleskaret, G.; Wright, C.M.; Power, G.F. The influence of contrast on coherent motion processing in dyslexia. *Neuropsychology* **2012**, *50*, 1672–1681. [CrossRef] [PubMed]
151. Mascheretti, S.; Gori, S.; Trezzi, V.; Ruffino, M.; Facoetti, A.; Marino, C. Visual motion and rapid auditory processing are solid endophenotypes of developmental dyslexia. *Genes Brain Behav.* **2018**, *17*, 70–81. [CrossRef] [PubMed]
152. Arslan, A. Genes, Brains, and Behavior: Imaging Genetics for Neuropsychiatric Disorders. *J. Neuropsychiatry Clin. Neurosci.* **2015**, *27*, 81–92. [CrossRef]
153. Franceschini, S.; Trevisan, P.; Ronconi, L.; Bertoni, S.; Colmar, S.; Double, K.; Facoetti, A.; Gori, S. Action video games improve reading abilities and visual-to-auditory attentional shifting in English-speaking children with dyslexia. *Sci. Rep.* **2017**, *7*, 1–12. [CrossRef]